Earth and Planetary Science Letters 428 (2015) 1–10

Contents lists available at ScienceDirect

Earth and Planetary Science Letters

www.elsevier.com/locate/epsl

Acquisition of chemical remanent magnetization during experimental ferrihydrite–hematite conversion in Earth-like magnetic field—implications for paleomagnetic studies of red beds

Zhaoxia Jiang [a], Qingsong Liu [a,*], Mark J. Dekkers [b], Lisa Tauxe [c], Huafeng Qin [a], Vidal Barrón [d], José Torrent [d]

[a] State Key Laboratory of Lithospheric Evolution, Institute of Geology and Geophysics, Chinese Academy of Sciences, Beijing 100029, China
[b] Department of Earth Sciences, Paleomagnetic Laboratory 'Fort Hoofddijk', Faculty of Geosciences, Utrecht University, Budapestlaan 17, 3584 CD Utrecht, The Netherlands
[c] Scripps Institution of Oceanography, University of California San Diego, San Diego, CA 92093-0220, USA
[d] Departamento de Agronomía, Universidad de Córdoba, Edificio C4, Campus de Rabanales, 14071 Córdoba, Spain

ARTICLE INFO

Article history:
Received 12 May 2015
Received in revised form 6 July 2015
Accepted 6 July 2015
Available online 24 July 2015
Editor: B. Buffet

Keywords:
hematite
crystal growth
chemical remanent magnetization (CRM)
detrital remanent magnetization (DRM)

ABSTRACT

Hematite-bearing red beds are renowned for their chemical remanent magnetization (CRM). If the CRM was acquired substantially later than the sediment was formed, this severely compromises paleomagnetic records. To improve our interpretation of the natural remanent magnetization, the intricacies of the CRM acquisition process must be understood. Here, we contribute to this issue by synthesizing hematite under controlled 'Earth-like' field conditions ($\lesssim$100 μT). CRM was imparted in 90 oriented samples with varying inclinations. The final synthesis product appeared to be dominated by hematite with traces of ferrimagnetic iron oxides. When the magnetic field intensity is $\gtrsim$40 μT, the CRM records the field direction faithfully. However, for field intensities $\lesssim$40 μT, the CRM direction may deviate considerably from that of the applied field during synthesis. The CRM intensity normalized by the isothermal remanent magnetization (CRM/IRM$_{@2.5\,T}$) increases linearly with the intensity of growth field, implying that CRM could potentially be useful for relative paleointensity studies if hematite particles of chemical origins have consistent properties. CRM in hematite has a distributed unblocking temperature spectrum from ~200 to ~650 °C, while hematite with a depositional remanent magnetization (DRM) has a more confined spectrum from ~600 to 680 °C because it is usually coarser-grained and more stoichiometric. Therefore, the thermal decay curves of CRM with their concave shape are notably different from their DRM counterparts which are convex. These differences together are suggested to be a potential discriminator of CRM from DRM carried by hematite in natural red beds, and of significance for the interpretation of paleomagnetic studies on red beds.

1. Introduction

Red beds, detrital sedimentary rocks pigmented by hematite, are widely distributed in tropical and subtropical areas (Robb, 1949; Walker, 1967; Van Houten, 1968, 1973; Collinson, 1974) and have been extensively used for paleomagnetic studies (Kent et al., 1986; Tan et al., 2003; Iosifidi et al., 2010). The natural remanent magnetization (NRM) in most red beds is a composite of detrital and authigenic hematite (Collinson, 1966, 1974; Tauxe et al., 1980). The authigenic hematite may have been formed long after deposition of the red bed and this chemical remanent magnetization (CRM) compromises a clear-cut interpretation of paleomagnetic records of red beds (Kent et al., 1987; McCabe and Elmore, 1989; Wang and Van der Voo, 1993; Elmore et al., 2006; Van der Voo and Torsvik, 2012). CRM usually overprints the primary remanent magnetization of red beds – a detrital remanent magnetization (DRM) – either partially or completely, and thus complicates paleomagnetic interpretations (Stearns and Van der Voo, 1987; Huang and Opdyke, 1996; Deng et al., 2007; Dekkers, 2012). Therefore, a central aspect of paleomagnetic studies on red beds is to discriminate CRM from DRM in order to discern the primary NRM component – if at all possible (e.g. Collinson, 1965; Kodama and Dekkers, 2004; Liu et al., 2011). To better appreciate the potential range of CRM behavior, the CRM acquisition process should be understood.

* Corresponding author. Tel.: +86 1082998365.
E-mail address: qsliu@mail.iggcas.ac.cn (Q. Liu).

http://dx.doi.org/10.1016/j.epsl.2015.07.024
0012-821X/

CRM is acquired during chemical change of minerals below their Curie or Néel temperatures in the presence of an ambient magnetic field. This occurs during weathering, diagenesis, or metamorphism. CRM formation can be the result of simple crystal growth (growth-CRM) or of the alteration of parent magnetic minerals (alteration-CRM) (e.g. Haigh, 1958; Stokking and Tauxe, 1990a). However, the acquisition of a stable CRM requires magnetic minerals of a certain minimal size larger than the superparamagnetic (SP) threshold size. Beyond this size range, changes in the external field direction and/or intensity have little or no effect on the remanent magnetization.

The CRM acquisition process in hematite has been simulated experimentally in the laboratory (Hedley, 1968; Bailey and Hale, 1981; Stokking and Tauxe, 1987, 1990a, 1990b; Özdemir and Dunlop, 1993; Gendler et al., 2005). Aspects of alteration-CRM were explored by Marshall and Cox (1971) who investigated the CRM of submarine basalt acquired through mineral transformation (titanomagnetite → titanohematite) during heating in an ambient field. They found that the direction of NRM was not affected by CRM acquisition if the oxidation occurs below the original Curie temperature of the titanomagnetite. However, Bailey and Hale (1981) determined that the CRM direction acquired by submarine basalts during heating in a laboratory field of 50 μT is between the ambient field direction and that of the pre-existing NRM. Özdemir and Dunlop (1993) studied the CRM accompanying the phase transformation lepidocrocite → maghemite → hematite in a field of 50 μT from 200 to 650 °C. They observed two CRM intensity peaks around 275 °C and 400 °C that were also detected by Gendler et al. (2005). The lepidocrocite → maghemite and maghemite → hematite transformations occur at these two respective temperatures.

For the understanding of growth-CRM the pathway of hematite formation is important. Hematite can crystallize through various pathways, directly from the hydrolysis of ferric iron salts (Schwertmann and Cornell, 2000) or indirectly via the ferrihydrite → hematite reaction (Schwertmann and Cornell, 2000) or the ferrihydrite → ferrimagnetic ferrihydrite (hydromaghemite) → hematite reaction chain (Barrón and Torrent, 2002; Barrón et al., 2003, 2012; Michel et al., 2010). To understand the properties of growth-CRM, Stokking and Tauxe (1987) synthesized hematite crystals in an aqueous ferric nitrate solution in magnetic fields controlled with three orthogonal sets of Helmholtz coils. They found that the CRM was acquired parallel to the applied field. In addition, its intensity was a linear function of the field up to 7.5 mT (Stokking and Tauxe, 1990a). However, when two perpendicular fields were applied during hematite growth in two different stages, the CRM behavior became complex (Stokking and Tauxe, 1990b). The resulting CRM could be parallel or antiparallel to, as well as intermediate between these two fields, underscoring the complexity inherent to the process of remanence acquisition by crystals precipitating from solution. Therefore, how to interpret CRM directions in terms of ancient field directions is not straightforward.

Previous studies investigated either processes at certain single field values or a large range of typically rather strong growth fields (~0–7.5 mT). No study has yet systematically investigated the properties of CRM acquired in fields similar to the Earth's magnetic field, which is more relevant for paleomagnetic studies of natural samples. In addition, the relationship of CRM intensity versus applied field has not been investigated systematically, apart from the study by Stokking and Tauxe (1990a). To study the behavior of CRM versus applied field under earth-like field conditions, we synthesized a series of hematite samples in $2 \times 2 \times 2$ cm^3 cubes. Ferrihydrite was transformed to hematite under controlled conditions (fields: ~10–100 μT, temperature: 95 °C). The CRM and other magnetic properties of these samples grown in different field strengths are reported here, and their paleomagnetic significance for red bed studies will also be discussed.

2. Sample preparation and methods

2.1. Sample preparation

Ferrihydrite was synthesized by mixing 100 mL 0.5 M Fe $(NO_3)_3$ and 100 mL of 2 M NaOH. Subsequently 50 mL 1 M $NaHCO_3$ was added to bring the pH to ~7. The deionized water for the solutions was heated to 90 °C in advance to inhibit the formation of goethite. The resulting brown ferrihydrite suspensions (the precursor of hematite) were centrifuged and the supernatant solution was preserved in a cylinder to age the ferrihydrite to hematite. To prevent DRM acquisition, the fresh ferrihydrite was mixed with quartz wool and then pressed into ceramic boxes ($2 \times 2 \times 2$ cm^3). The quartz wool and ceramic boxes were thermally demagnetized to 700 °C before being used in order to remove any remanence. The cubic ceramic samples were given an orientation line to be able to retain the orientation in subsequent sample manipulations and mounted in the cylinder containing the supernatant. The ferrihydrite was aged under controlled temperature and field conditions. The temperature of the solution was maintained at 95 ± 3 °C by a small furnace equipped with a digital thermometer. A controlled magnetic field was obtained with two sets of Helmholtz coils (1 m × 1 m) which were aligned with the declination of the ambient field in the laboratory. One pair of coils was set horizontal to produce the vertical field component, while the other pair was put vertical to produce the horizontal component. In this manner CRMs with (nearly) zero declination and any desired inclination can be imparted. The iron oxides were grown in nine different magnetic field strengths; the directions and strengths are summarized in Table 1. For each field setting, twelve samples were obtained. The sample series are labeled CRM1* (100.8 μT), CRM2* (85.7 μT), CRM3* (67.6 μT), CRM4* (54.7 μT), CRM5* (44.2 μT), CRM6* (37.9 μT), CRM7* (24.2 μT), CRM8* (16.2 μT), and CRM9* (11.9 μT). The aging was almost completed in two weeks as confirmed by a trial experiment with susceptibility measurement made every day. Thereafter the samples were dried and cooled in a field-free space to avoid the acquisition of a partial thermal remanent magnetization (pTRM). The dried samples were kept in a magnetically shielded room with residual field <300 nT prior to making the magnetic measurements.

2.2. Experimental methods

The anisotropy of magnetic susceptibility (AMS) of these samples was first measured using an AGICO KLY-4S Kappabridge. The remanent magnetizations were measured with a cryogenic magnetometer system (2G Enterprises 760R) installed in the magnetically shielded room with residual field <300 nT. Firstly, all the samples were subjected to progressive alternating field (AF) demagnetization to resolve a possible soft remanence component in the samples, i.e., potential contamination of maghemite or ferrimagnetic ferrihydrite. Then each sample series was divided into two groups; one group of samples was used to measure the isothermal remanent magnetization acquired at 2.5 T field ($IRM_{@2.5\,T}$), and the other group of samples was subjected to stepwise thermal demagnetization from 80 °C to a maximum temperature of 700 °C with 10 °C intervals between 80 and 150 °C and between 600 and 700 °C to precisely resolve potential goethite and hematite remanences respectively. Between 150 and 600 °C the demagnetization interval was 50 °C. A Magnetic Measurements thermal demagnetizer with a residual magnetic field <10 nT was used for this purpose.

Table 1
Summary of the field conditions in the chemical remanent magnetization experiments. CRM is the remanence measured after the growth experiment and ChRM the remanence measured after thermal demagnetization between 200 and 640 °C.

Sample series	Applied field			CRM			ChRM		
	Declination	Inclination	Intensity (μT)	Declination	Inclination	Deviation (ΔD/ΔI)	Declination	Inclination	Deviation (ΔD/ΔI)
CRM1	5.9	−42.2	100.8	1.6	−35.5	−4.3/6.7	−0.5	−29.5	−6.4/12.7
CRM2	4.5	−48.5	85.7	2.95	−41	1.55/7.5	No thermal demagnetization		
CRM3	9.4	−53.7	67.6	6.6	−40.3	−2.8/13.4	2.9	−38.5	6.5/15.2
CRM4	3	48.9	54.7	8.8	34.3	5.8/−14.6	No thermal demagnetization		
CRM5	2.7	36.2	44.2	8.3	36.8	−5.6/0.6	No thermal demagnetization		
CRM6	−15.4	−41.2	37.9	1.9	−28.3	17.3/12.9	2.2	−34.7	17.6/6.5
CRM7	−3.4	33.8	24.2	11.1	47	14.5/13.2	No thermal demagnetization		
CRM8	−26.5	−38.1	16.2	27.3	−78.6	53.8/40.5	43.7	−79.7	70.2/41.6
CRM9	−10	51.4	11.9	40.7	65	50.7/13.6	No thermal demagnetization		

The samples that were subjected to the $IRM_{@2.5\,T}$ measurement were removed from the ceramic boxes afterwards for additional rock magnetic measurements. Samples were ground to powder and then sieved with a 200 mesh sieve to remove the quartz wool. Firstly, IRM acquisition curves with 80 steps were measured with a maximum field 2 T on a Princeton Measurements Corporation vibrating sample magnetometer (Micromag VSM 3900) at room temperature. The IRM acquisition curves were decomposed into magnetic coercivity components using the method of Kruiver et al. (2001) that works with the premise that the measured IRM acquisition curves can be represented by a linear addition of coercivity components represented by cumulative log-Gaussian functions. Subsequently, the back-field curves were measured to determine remanent coercivity (B_{cr}). Hysteresis loops for all these samples were measured at room temperature in 5 mT increments using a Micromag VSM 3900 with a maximum field of 2 T. Finally, thermomagnetic curves in a steady field of 1 T (J–T) curve were measured from room temperature to 800 °C in air, using a Magnetic Measurements Variable Field Translation Balance (VFTB).

3. Results

3.1. Characterization of growth material

X-ray diffractograms (XRD) of the powder samples (Fig. 1) showed the presence of hematite. But the dominant mineral, appeared to be sodium nitrate ($NaNO_3$) because the supernatant solution contained mainly Na^+, NO_3^- and HCO_3^-.

As shown by the J–T curves of selective samples (Fig. 2, left most column of panels), no clear Néel temperature of hematite can be observed and the J–T curves display a hyperbolic shape, which is interpreted to be due to the dominant effects of superparamagnetic (SP) minerals. The cooling branches are lower than the corresponding heating branches for all samples which may be the result of grain growth or 'crystal healing' of these samples during the thermomagnetic experiment. Hysteresis loops (Fig. 2, left-central column of panels) and IRM acquisition curves (Fig. 2, right-central column of panels) show that these samples are far from being saturated even in a 2 T field, so B_{cr} acquired from back field curves is a minimum estimate. Hysteresis loops exhibit a ramp-like shape, demonstrating the presence of SP particles. In addition, the IRM component analyses (Fig. 2, right-most column of panels) indicate the presence of two magnetic components, a relatively low coercivity (L) component with a mean coercivity ($B_{1/2L}$) ranging between 22∼40 mT, and a high coercivity (H) component with a mean coercivity ($B_{1/2H}$) larger than 1 T (see also Table 2). The IRM of these samples appears to be dominated by the high coercivity component which contributes from 85 to 98% of the IRM (Table 2). B_{cr} decreases with decreasing growth field (except for the CRM6* series grown in a field of 37.9 μT), which is consistent with the variation trend of $B_{1/2H}$.

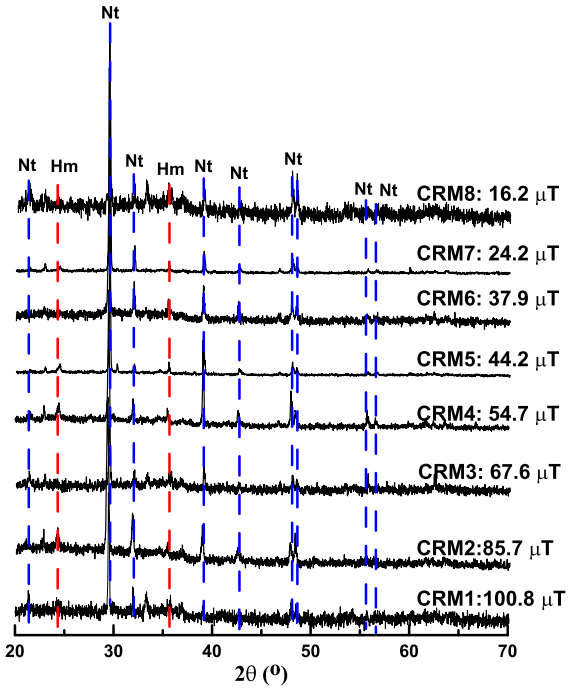

Fig. 1. X-ray diffractograms of samples grown in different applied magnetic fields. The red and blue lines represent the characteristic reflections of hematite and sodium nitrate ($NaNO_3$), respectively, where Hm and Nt are the abbreviations of hematite and sodium nitrate. (For interpretation of the references to color in this figure legend, the reader is referred to the web version of this article.)

3.2. CRM characterization

The AMS results of the oriented samples are barely above the instrument noise level. The representative four series of samples have very low anisotropy degrees (P) with the majority being <1.01 without a tendency for oblate or prolate shapes (Fig. 3). Each component of magnetic susceptibility is distributed randomly in equal area projection, so the growth field does not impact the orientation of the AMS tensor.

AF demagnetization up to 100 mT of these samples typically removes less than 20% of CRM (Fig. 4), indicating that they are magnetically hard and only slightly contaminated (if at all) with ferrimagnetic phases, which can be an intermediate product in the transformation of ferrihydrite to hematite (Cabello et al., 2009; Michel et al., 2010). After AF demagnetization, the samples were subjected to progressive stepwise thermal demagnetization: the CRM decays univectorially to the origin (Fig. 5). The characteristic remanent magnetization (ChRM) can be isolated between 200 and 640 °C, demonstrating that pigmentary hematite is the major magnetic carrier. An inflection can be detected around 300 °C

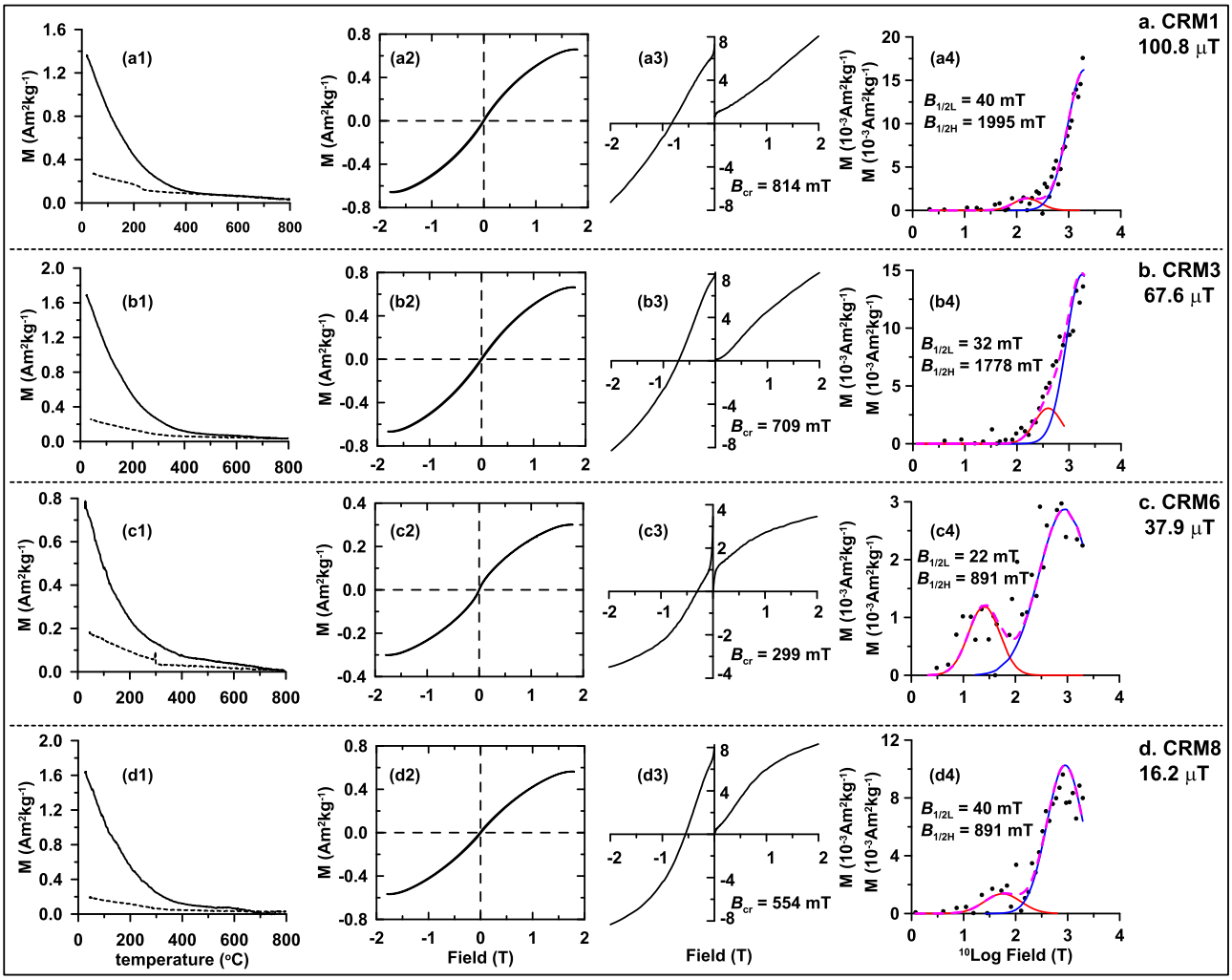

Fig. 2. The rock magnetic properties of some representative samples. (a1, b1, c1, d1) Thermomagnetic curves (J–T) in air, where the solid and dashed lines are the heating and cooling branches. (a2, b2, c2, d2) Hysteresis loops. The two left-handed columns of panels do not indicate the remanent magnetization directly but demonstrate the presence of SP particles. (a3, b3, c3, d3) Acquisition curves of isothermal ramanent magnetization (IRM) and back-field demagnetization curves. (a4, b4, c4, d4) IRM component analysis, where the red, blue, and purple lines indicate the low coercivity, high coercivity components and the sum of these components. The solid points represent the raw IRM gradient data. (For interpretation of the references to color in this figure legend, the reader is referred to the web version of this article.)

Table 2
IRM component analysis of representative CRM samples (cf. Kruiver et al., 2001). $B_{1/2L}$ and $B_{1/2H}$ are the $B_{1/2}$ (mT) (the medium field at which half of the IRM is reached) of the low and high coercivity component, DP is the dispersion parameter of each IRM component. The IRM contribution (%) is the contribution of each IRM component to the total IRM.

Sample name	Component L			Component H		
	$B_{1/2L}$ (mT)	DP	IRM contribution (%)	$B_{1/2H}$ (mT)	DP	IRM contribution (%)
CRM1	40	0.26	5	1995	0.40	95
CRM3	32	0.2	2	1778	0.45	98
CRM6	22	0.25	15	891	0.55	85
CRM8	40	0.30	9	891	0.40	91

which may be the consequence of intermediate ferrimagnetic ferrihydrite transforming to hematite or the dehydration of hydrohematite around 300 °C. The wide range of blocking temperatures can be attributed to a varying particle size distribution. The remanence residing in the synthetic hematite after thermal demagnetization to 200 °C, is indeed a CRM.

The directions of the initial CRM, ChRM, and their growth fields are plotted on an equal area stereographic projection in Fig. 6. After the initial CRM measurements, each series of samples was divided into two groups, so the number of ChRM data points is less than that of the initial CRM directional data. Results show that for samples grown in fields $\gtrsim$40 μT, the field direction, CRM and ChRM directions are almost overlapping, that is, CRM records the applied field direction faithfully. For samples grown in fields $\lesssim$40 μT, however, the CRM direction notably deviates from that of applied field, especially for samples grown in fields $\lesssim$20 μT with deviations in direction larger than ~40° (Fig. 6 and Table 1).

The intensity of CRM versus the growth field plot in the range of 0 to ~100 μT (Fig. 7a) is rather scattered, showing only a broad intensity increase with the applied field. The CRM intensity of our samples ranges from 1 to 16×10^{-8} A m^2, but the CRM intensities for samples growing in the same field are quite dispersed, especially for samples produced in a field of 100.8 μT

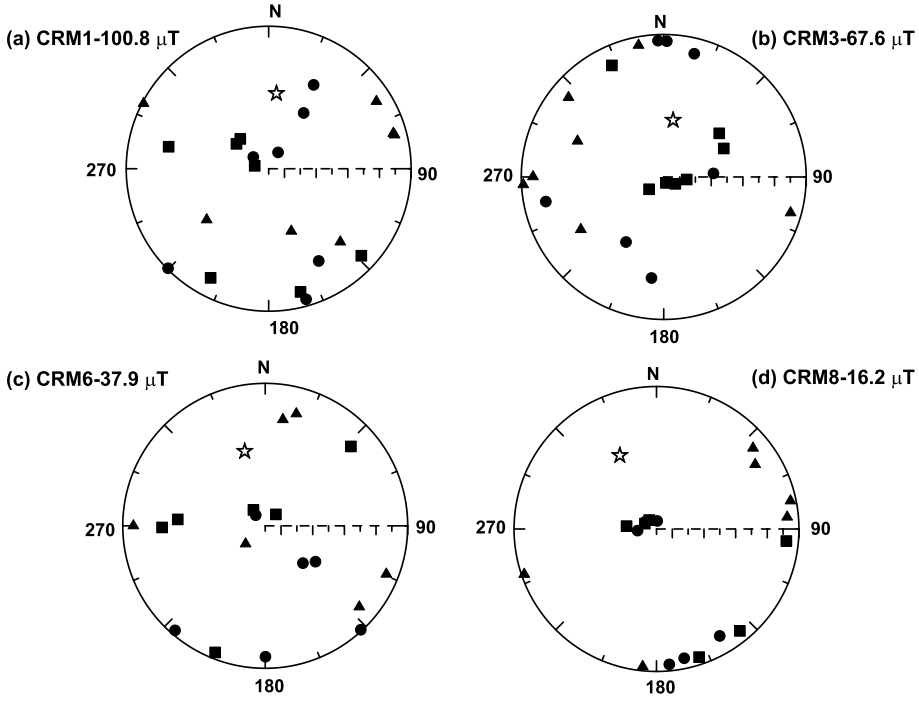

Fig. 3. The anisotropy of magnetic susceptibility (AMS) of samples grown in different applied magnetic fields, where the squares, triangles, and circles represent the maximum magnetic susceptibility (K_{max}), the intermediate magnetic susceptibility (K_{int}), and the minimum magnetic susceptibility (K_{min}) axes, respectively. The stars indicate the direction of the applied magnetic field during CRM acquisition.

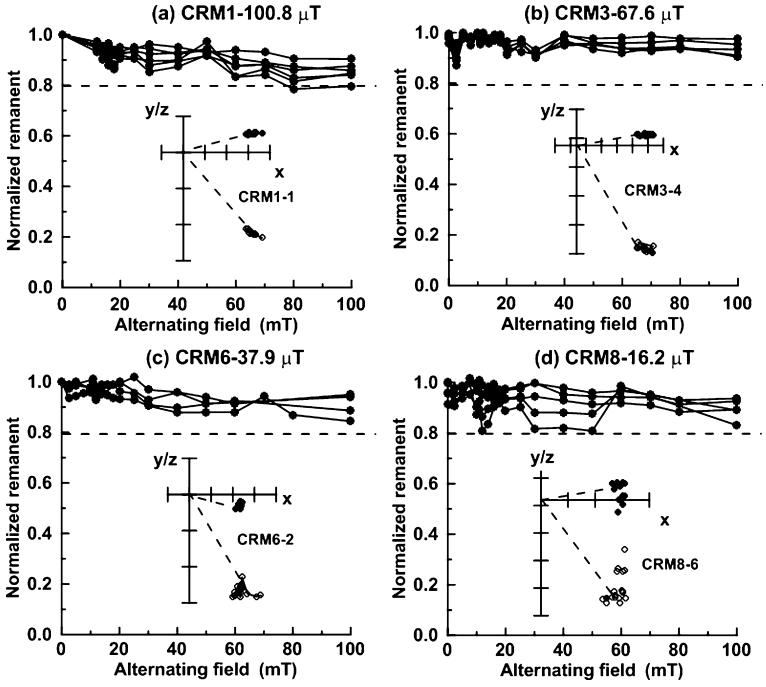

Fig. 4. Alternating field (AF) demagnetization curves of chemical remanent magnetization (CRM) for the series of samples: (a) CRM1-100.8 μT, (b) CRM6-67.6 μT, (c) CRM6-37.9 μT and (d) CRM8-16.2 μT. The insets show the orthogonal projections of progressive AF demagnetization for representative samples. The solid and open circles represent the horizontal and vertical projections, respectively.

which show intensity deviations up to 25%. Since it is difficult to quantify the hematite concentration in each sample, the CRM was normalized by $IRM_{@2.5\,T}$ for each individual sample to exclude the influence of mass difference (Fig. 7b). CRM intensity appears to be 2–12‰ of that of $IRM_{@2.5\,T}$. The value of $CRM/IRM_{@2.5\,T}$ increases linearly with the growth field, which is consistent with the results of Stokking and Tauxe (1990a).

4. Discussion

4.1. Characterization of final material

For the ferrihydrite → ferrimagnetic ferrihydrite → hematite transformation route, the final product will depend on the aging time (Barrón and Torrent, 2002; Michel et al., 2010). If the

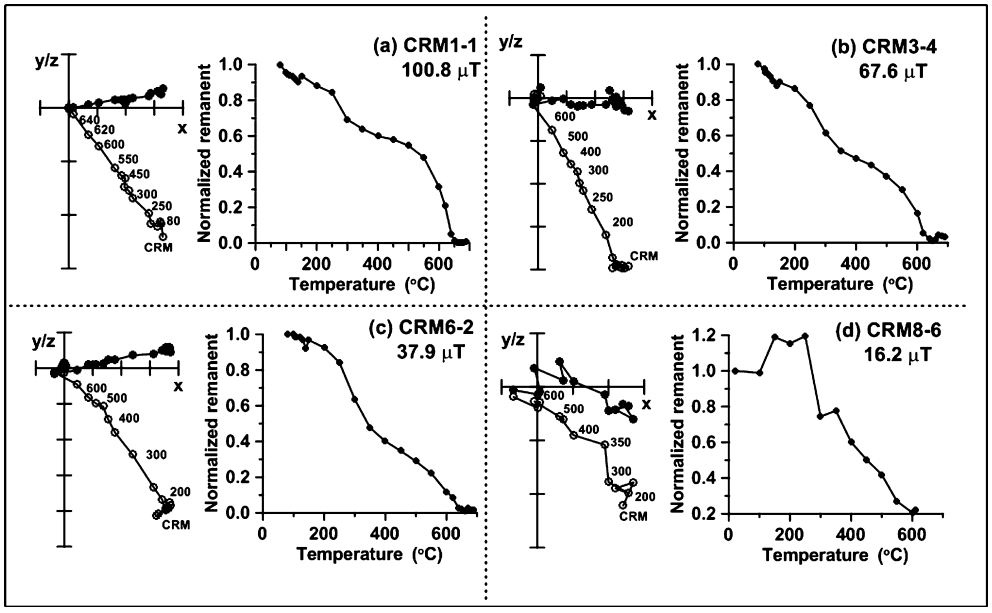

Fig. 5. Representative orthogonal projections of stepwise thermal demagnetization of chemical remanent magnetization (CRM) after AF demagnetization. (a) CRM1-1; (b) CRM3-4; (c) CRM6-2; and (d) CRM8-6. In the left-handed panels, the solid and open circles represent the horizontal and vertical projections, respectively. The decay curves normalized to the starting CRM intensity after the AF demagnetization are shown in the right-handed panels.

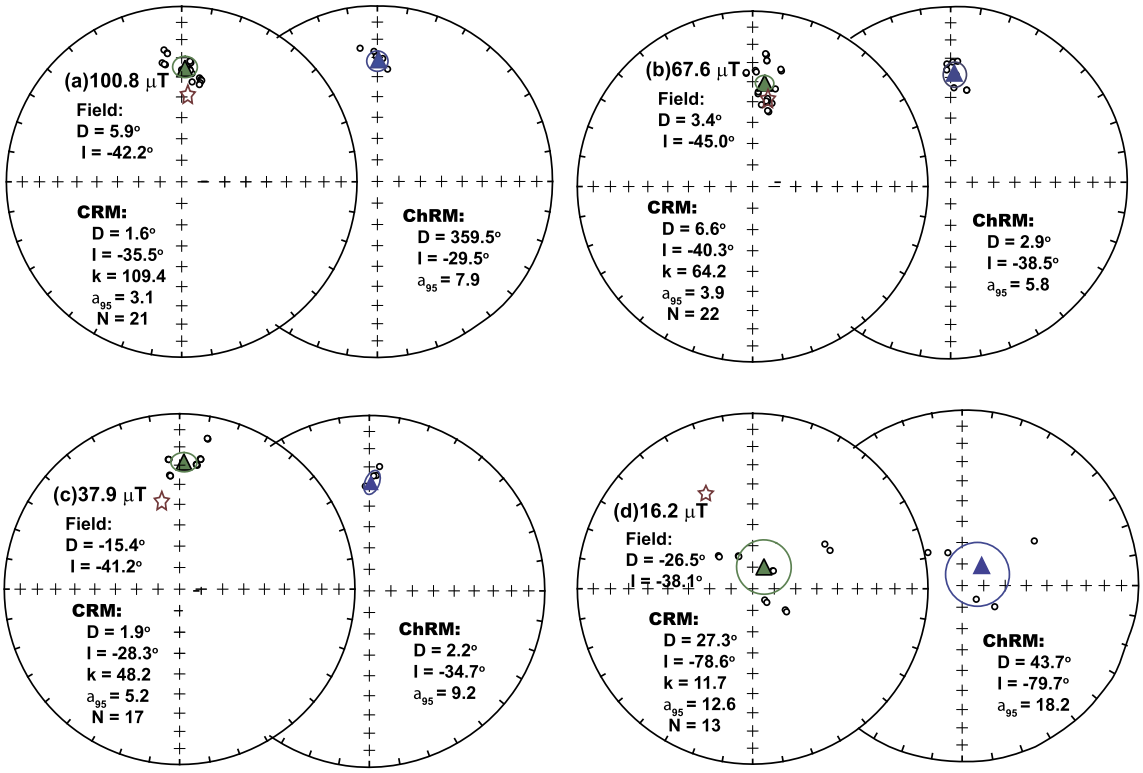

Fig. 6. Equal area projections of the directions of the starting chemical remanent magnetization (CRM), applied magnetic field (red star), and characteristic remanent magnetization (ChRM) retrieved after stepwise thermal demagnetization. The green and blue triangles show the mean directions of CRM and ChRM, ellipsoids represent the 95% confidence limits. (For interpretation of the references to color in this figure legend, the reader is referred to the web version of this article.)

aging time is not sufficiently long to complete the reaction, the samples are usually composed of SD hematite and intermediate products (ferrimagnetic ferrihydrite), both mostly as SP particles (Liu et al., 2008). The ramp-like hysteresis loops of our samples confirm the existence of finer magnetic particles. However, these SP particles cannot contribute to remanence. The IRM spectrum analysis shows that only two coercivity components can be detected, an "L" component with $B_{1/2L}$ around 22–40 mT and an "H" component with $B_{1/2H}$ around 1–2 T. Since no goethite signal can be observed during the thermal demagnetization process, the H component is then interpreted to be hematite, while the L component may be caused by the fine-grained ferrimagnetic ferrihydrite, which contributes less than 20% IRM, consistent with the AF demagnetization behavior of the CRM. In addition, as our samples

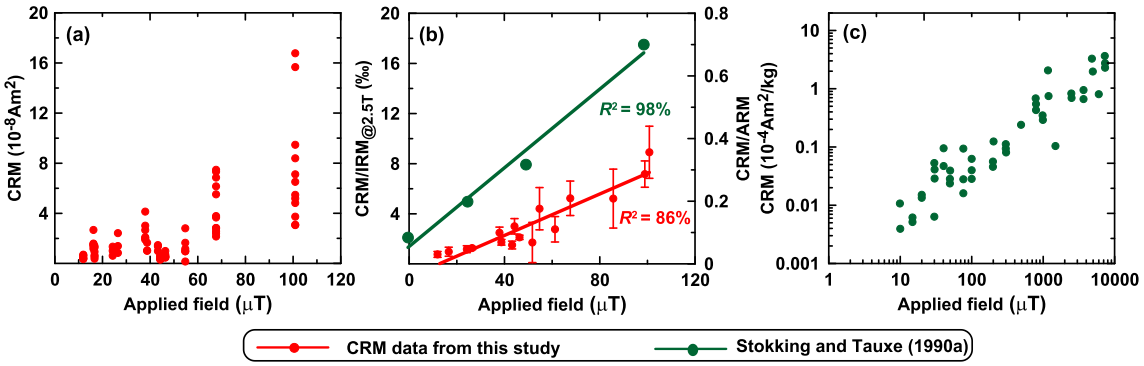

Fig. 7. Diagrams of chemical remanent magnetization (CRM) intensity versus applied field. (a) the original data of CRM intensity versus applied field for our data set; (b) CRM/IRM$_{@2.5\,T}$ (red: our data, IRM$_{@2.5\,T}$, isothermal remanent magnetization acquired at 2.5 T field) or CRM/ARM (green; data from Stokking and Tauxe, 1990a) versus applied field; (c) CRM data from Stokking and Tauxe (1990a) versus applied field (10–7500 μT). (For interpretation of the references to color in this figure legend, the reader is referred to the web version of this article.)

aged in the supernatant solution containing $NaNO_3$ and $NaHCO_3$, the final dry samples should include abundant crystalline $NaNO_3$, a notion confirmed by the XRD results (Fig. 1).

4.2. The dependence of CRM on the applied magnetic field

The relationship between growth CRM and the applied magnetic field is described by the following equations (Stacey and Banerjee, 1974; Stokking and Tauxe, 1990a),

$$\boldsymbol{M}_{CRM} = M_s \boldsymbol{B} \int_0^{\frac{\pi}{2}} \tanh \frac{m_b \cos\theta}{k} T \cos\theta \sin\theta d\theta \quad (1)$$

$$\frac{\boldsymbol{M}_{CRM}}{M_s} = \boldsymbol{B} \int_0^{\frac{\pi}{2}} \tanh \frac{m_b \cos\theta}{k} T \cos\theta \sin\theta d\theta \quad (2)$$

where M_s is the saturation magnetization at the temperature of CRM acquisition, m_b is the grain moment at the blocking volume, $\boldsymbol{B}$ is the magnetic field, and θ is the angle between the applied field and the "easy" direction of the grain. It follows from these equations that growth-CRM should be parallel to the applied magnetic field. The "normalized" CRM intensity, i.e. CRM intensity divided by M_s, is proportional to the applied magnetic field under the proviso that M_s and m_b remain constant (Stokking and Tauxe, 1990a; McClelland, 1996).

As expected from theory, no inclination shallowing occurs in CRM. Our results show that the CRM directions of hematite closely track the growth field orientation when the magnetic field intensity is higher than ~40 μT (Fig. 6), which is consistent with Stokking and Tauxe (1987). However, previous studies show that DRM carried by detrital hematite can suffer from serious inclination shallowing which can complicate the interpretation of paleomagnetic results from red beds (e.g., Tauxe and Kent, 1984; Tan et al., 2007; Bilardello and Kodama, 2010). Hence, CRM recorded shortly after deposition can record the direction of the actual magnetic field and is more suitable for paleomagnetic studies than DRM (Tauxe and Kent, 2004; Mitra and Tauxe, 2009; Iosifidi et al., 2010). However, when the applied field is less than ~40 μT, our synthesis products do not track the applied field and deviate from the field (Fig. 6c–d). This may be due to the synthesis route of the hematite from ferrihydrite, which mainly involves dehydration and solid-state rearrangement but not dissolution followed by precipitation. Alternatively, this could be simply caused by the inefficient alignment of the hematite magnetization at such lower applied fields. So it could be speculatively suggested that the packing of the ferrihydrite flocs plays a role in the low-field end of the experiments. It means that CRM formed in low fields may not record the geomagnetic field direction faithfully. This may be an underappreciated source of uncertainty in paleomagnetic studies of red beds. Some sites in magnetostratigraphic studies in red beds (not close to reversals) appear to deliver randomly oriented directions, particularly in paleosols (e.g., Tauxe and Opdyke, 1982), which could be due to the fact that CRM does not faithfully records field directions in weak magnetic fields (e.g., $\lesssim$40 μT).

Stokking and Tauxe (1990a) synthesized a series of CRM bearing samples and demonstrated that CRM intensity was nearly linearly related to the applied field intensity from 0.015 mT to 7.5 mT (Fig. 7c). However, the geomagnetic field intensity is nearly always <100 μT (e.g. Tauxe et al., 2013). So CRMs acquired in fields of <100 μT is more relevant for paleomagnetic studies. Therefore, we compare our results from 10 to 100 μT with those from Stokking and Tauxe (1990a). We normalize the CRM with IRM$_{@2.5\,T}$ for our samples (CRM/IRM$_{@2.5\,T}$) to compare with the CRM data normalized by ARM (CRM/ARM) from Stokking and Tauxe (1990a). The CRM/IRM$_{@2.5\,T}$ or CRM/ARM increases linearly with the applied field from ~0 to 100 μT (Fig. 7b), which is in accordance with the theoretical equations.

Although some other magnetic minerals could be present in trace amounts in the final synthesis product, thermal demagnetization curves of the oriented samples demonstrate that hematite is the dominant magnetic remanence carrier. Therefore, CRM of hematite can record the geomagnetic field intensity faithfully. In other words, CRM recorded by hematite can in principle be used for relative paleointensity studies in the earth-like field range. However, for the interpretation of CRM records in terms of relative paleointensity the prolonged growth of CRM in nature should be considered. This (yet undefined) timespan of growth implies that such red bed relative intensity records represent a certain time-averaged field; they average out short-lived intensity peaks and troughs. Also multiple growth stages complicate interpretation as indicated by results of Stokking and Tauxe (1990b). The classic scanning electronic microscopy study of hematite in the Moenkopi Formation (USA) shows multiple periods of secondary hematite growth (Walker et al., 1981). So, for a meaningful interpretation of red bed CRM in terms of relative paleointensity, a dominant growth phase that can be tied to early diagenesis should be established.

4.3. Discrimination of CRM and DRM of red beds

Two kinds of hematite, black (specular) grains and red pigment, are known in soils and red beds. Fine-grained chemically formed hematite is responsible for the characteristic color of red beds and

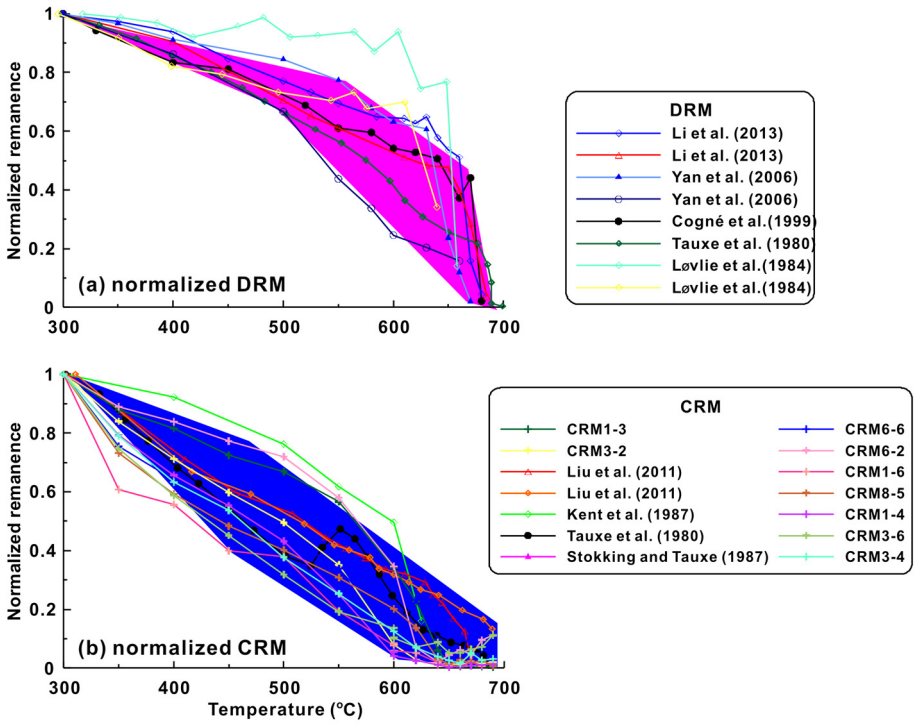

(c) Summary of reference data used in this figure

Reference	locality	mineralogy	age	remanent type
Tauxe et al. (1980)	Middle Siwalik	Hematite pigment, specular hematite	Miocene	CRM & DRM
Kent et al. (1987)	Yichang, China	hematic sandstone	upper Devonian	CRM
Stokking & Tauxe (1987)	grown in the laboratory	hematite pigment		CRM
Cogné et al. (1999)	Qiangtang block of Tibet	red sandstone	Eocene	DRM
Løvlie et al. (1984)	North Central Spitsbergen	sandstone composed of hematite granules	Devonian	DRM
Yan et al. (2006)	Gonghe-GuideBasin	mudstones and siltstones	Miocene	DRM
Liu et al. (2011)	Yunnan province	Limestones interbedded with mudstones and sandstones	uppermost Permian	CRM

Fig. 8. Stepwise thermal demagnetization curves of (a) detrital remanent magnetization (DRM) and (b) chemical remanent magnetization (CRM) for our samples and some reference data; (c) summary of the reference data used in this figure. Data were normalized at the 300 °C step to remove the influence of potentially present viscous remanent magnetization. The pink and blue fields indicate the general shapes of the DRM and CRM demagnetization curves. (For interpretation of the references to color in this figure legend, the reader is referred to the web version of this article.)

are the dominant magnetic carrier in some red beds in warm and humid climates (Robb, 1949; Walker, 1967; Van Houten, 1968; Torrent and Schwertmann, 1987). Detrital hematite, black specularite, is frequently coarser-grained. Tauxe et al. (1980) identified these two kinds of hematites in the Siwalik red beds. The red pigment had a lower and comparatively broad blocking temperature spectrum and higher coercivity, while the black hematite had higher blocking temperatures and lower coercivity. The former can be removed by chemical dissolution and was interpreted to record a chemical remanent magnetization, while the latter most likely carried a detrital remanent magnetization (Tauxe et al., 1980). However, a near-primary origin of a CRM can record the direction of the magnetic field faithfully. If the field strength is sufficiently strong, such remanences are also useful for paleomagnetic reconstruction (Iosifidi et al., 2010). Kodama (2012) suggested that a criterion to discriminate DRM and CRM would be whether or not the red beds suffer from inclination shallowing. However, when the prevailing DRM is overprinted by CRM, it is difficult to interpret the resulting magnetization as reflecting the actual recording of the geomagnetic field (McCabe and Elmore, 1989; Deng et al., 2007) since the resultant magnetization is a convolved DRM and CRM. As a result, a more robust means of separating DRM from CRM is indispensable.

McClelland-Brown (1982) successfully used the blocking temperature spectrum to discriminate TRM and CRM in hematite. Inspired by this result, we summarized the stepwise thermal demagnetization curves of our data and previous results in Fig. 8, where all the data were normalized by the remanence after demagnetization at 300 °C to remove the influence of viscous remanent magnetization. Our investigations show that the CRM in our samples is completely demagnetized around 600 to 650 °C which is considered to be the maximum unblocking temperature for our samples (Fig. 8b). However, most of the DRM continues to unblock to temperatures up to 660–680 °C (Tauxe et al., 1980; Løvlie et al., 1984; Cogné et al., 1999; Yan et al., 2006; Li et al., 2013), distinctly higher than that of our CRM (Fig. 8). Apparently, CRM has a more distributed unblocking temperature spectrum (~200 to 600–650 °C) than DRM (mostly 600–680 °C). These differences in blocking temperature between CRM and DRM can be attributed to differences in grain size and crystallinity. The DRM of red beds is usually carried by detrital hematite particles with a larger particle size (Collinson, 1965; Steiner, 1983; Tauxe and Kent, 1984), while CRM is carried by newly-formed fine-grained hematite pigment (Collinson, 1966; Tauxe et al., 1980; McClelland-Brown, 1982). Since the blocking temperature is positively related to the particle size of magnetic minerals in the single domain state based on Néel theory (O'Reilly, 1984; Dunlop and

Özdemir, 2001), the maximum unblocking temperature of specular hematite (DRM) is higher than that of the pigmentary hematite (CRM). In addition, the decay curves display different shapes. Summarizing the results from previous studies, DRM demagnetization curves appear to have a convex shape and drop to zero around 670–680 °C (Fig. 8a), which is supported by data shown in Kodama (2012, his Fig. 6.2). The demagnetization curves of CRM display a concave shape and decay to zero gradually (Fig. 8b). These distinct differences may be used to distinguish CRM from (most of the) DRM in red beds. Although the unblocking temperature spectrum of CRM recorded in very coaser particles will overlap with that of DRM and complicate their distinction as NRM components (Whidden et al., 1998), our observation can still be used as a secondary, supporting line of evidence to discriminate the CRM and DRM in red beds.

5. Conclusions

In this study, a growth-CRM was imparted in 90 oriented cubic samples ($2 \times 2 \times 2$ cm^3) synthesized in different applied magnetic fields ($\lesssim$100 μT) to investigate the CRM acquisition and properties of the resulting magnetic minerals. The final synthetic magnetic products are a mixture of hematite and ferrihydrite or maghemite.

The CRM directions for these oriented samples closely follow that of the growth field when the field is above ∼40 μT, however, CRM does not faithfully record the field direction once the field is lower than ∼40 μT. The normalized intensity of CRM (CRM/IRM$_{@2.5T}$) is linearly related with the applied magnetic field according to theory prediction. Therefore, CRM recorded by hematite can in principle be used for relative paleointensity studies in earth-like field ranges, however, some caution is appropriate as CRM directions may be poorly constrained in low fields.

The different blocking temperature spectrum can be used to discriminate CRM (gradual decay between ∼200 and 650 °C) and DRM (most decay in the 600–680 °C range) in red beds. Further, thermal demagnetization curves of CRM have a concave shape while those of a DRM are convex in shape. This is a potential discriminator of CRM from DRM carried by hematite in natural media, and is significant for paleomagnetic studies of red beds.

Acknowledgements

Dr. Greig Paterson is thanked for meaningful discussion on the experiments. Han Peng and Su Kai are thanked for their help during CRM experiments. This study was supported by the National Natural Science Foundation of China (grants 41430962, 41374073, and 41025013), Chinese Continental Shelf Deep Drilling Program (GZH201100202), and GASI-GEOGE-03. Z.X. Jiang further acknowledges support from the China Postdoctoral Science Foundation. L. Tauxe acknowledges support from the NSF (EAR1345003).

References

Bailey, M.E., Hale, C.J., 1981. Anomalous magnetic directions recorded by laboratory-induced chemical remanent magnetization. Nature 294, 739–741.
Barrón, V., Torrent, J., 2002. Evidence for a simple pathway to maghemite in Earth and Mars soils. Geochim. Cosmochim. Acta 66, 2801–2806.
Barrón, V., Torrent, J., De Grave, E., 2003. Hydromaghemite, an intermediate in the hydrothermal transformation of 2-line ferrihydrite into hematite. Am. Mineral. 88, 1679–1688.
Barrón, V., Torrent, J., Michel, F.M., 2012. Critical evaluation of the revised akdalaite model for ferrihydrite—discussion. Am. Mineral. 97, 253–254.
Bilardello, D., Kodama, K.P., 2010. Rock magnetic evidence for inclination shallowing in the early Carboniferous Deer Lake Group red beds of western Newfoundland. Geophys. J. Int. 181 (1), 275–289.
Cabello, E., Morales, M., Serna, C., Barrón, V., Torrent, J., 2009. Magnetic enhancement during the crystallization of ferrihydrite at 25 and 50 °C. Clays Clay Miner. 57, 46–53.
Cogné, J., Halim, N., Chen, Y., Courtillot, V., 1999. Resolving the problem of shallow magnetizations of Tertiary age in Asia: insights from paleomagnetic data from the Qiangtang, Kunlun, and Qaidam blocks (Tibet, China), and a new hypothesis. J. Geophys. Res. 104, 17715–17734.
Collinson, D., 1965. The remanent magnetization and magnetic properties of red sediments. Geophys. J. R. Astron. Soc. 10, 105–126.
Collinson, D., 1966. Carrier of remanent magnetization in certain red sandstones. Nature 210, 516–517.
Collinson, D., 1974. The role of pigment and specularite in the remanent magnetism of red sandstones. Geophys. J. R. Astron. Soc. 38 (2), 253–264.
Dekkers, M.J., 2012. End-member modelling as an aid to diagnose remagnetization: a brief review. Geol. Soc. (Lond.) Spec. Publ. 371 (1), 253–269.
Deng, C., Liu, Q., Wang, W., Liu, C., 2007. Chemical overprint on the natural remanent magnetization of a subtropical red soil sequence in the BoseBasin, southern China. Geophys. Res. Lett. 34, L22308. http://dx.doi.org/10.1029/22007GL031400.
Dunlop, D.J., Özdemir, Ö., 2001. Rock Magnetism: Fundamentals and Frontiers. Cambridge University Press, Cambridge, United Kingdom.
Elmore, R.D., Dulin, S., Engel, M.H., Parnell, J., 2006. Remagnetization and fluid flow in the old red sandstone along the Great Glen Fault, Scotland. J. Geochem. Explor. 89, 96–99.
Gendler, T.S., Shcherbakov, V.P., Dekkers, M.J., Gapeev, A.K., Gribov, S.K., McClelland, E., 2005. The lepidocrocite–maghemite–haematite reaction chain—I. Acquisition of chemical remanent magnetization by maghemite, its magnetic properties and thermal stability. Geophys. J. Int. 160, 815–832.
Haigh, G., 1958. The process of magnetization by chemical change. Philos. Mag. 3, 267–286.
Hedley, I., 1968. Chemical remanent magnetization of the FeOOH, Fe_2O_3 system. Phys. Earth Planet. Inter. 1, 103–121.
Huang, K., Opdyke, N.D., 1996. Severe remagnetization revealed from Triassic platform carbonates near Guiyang, Southwest China. Earth Planet. Sci. Lett. 143, 49–61.
Iosifidi, A.G., Mac Niocaill, C., Khramov, A.N., Dekkers, M.J., Popov, V.V., 2010. Palaeogeographic implications of differential inclination shallowing in Permo-Carboniferous sediments from the Donets basin, Ukraine. Tectonophysics 490, 229–240.
Kent, D.V., Xu, G., Huang, K., Zhang, W., Opdyke, N.D., 1986. Paleomagnetism of upper Cretaceous rocks from South China. Earth Planet. Sci. Lett. 79 (1), 179–184.
Kent, D.V., Zeng, X., Zhang, W.Y., Opdyke, N.D., 1987. Widespread late Mesozoic to recent remagnetization of Paleozoic and lower Triassic sedimentary rocks from South China. Tectonophysics 139, 133–143.
Kodama, K., 2012. Paleomagnetism of Sedimentary Rocks: Process and Interpretation. John Wiley & Sons.
Kodama, K., Dekkers, M.J., 2004. Magnetic anisotropy as an aid to identifying CRM and DRM in red sedimentary rocks. Stud. Geophys. Geod. 48, 747–766.
Kruiver, P.P., Dekkers, M.J., Heslop, D., 2001. Quantification of magnetic coercivity components by the analysis of acquisition curves of isothermal remanent magnetization. Earth Planet. Sci. Lett. 189, 269–276.
Li, S., Deng, C., Yao, H., Huang, S., Liu, C., He, H., Pan, Y., Zhu, R., 2013. Magnetostratigraphy of the Dali Basin in Yunnan and implications for late Neogene rotation of the southeast margin of the Tibetan Plateau. J. Geophys. Res. 118, 791–807.
Liu, C., Ge, K., Zhang, C., Liu, Q., Deng, C., Zhu, R., 2011. Nature of remagnetization of Lower Triassic red beds in southwestern China. Geophys. J. Int. 187, 1237–1249.
Liu, Q.S., Barron, V., Torrent, J., Eeckhout, S., Deng, C.L., 2008. Magnetism of intermediate hydromaghemite in the transformation of 2-line ferrihydrite into hematite and its paleoenvironmental implications. J. Geophys. Res. 113, B01103. http://dx.doi.org/10.1029/2007JB005207.
Løvlie, R., Torsvik, T., Jelenska, M., Levandowski, M., 1984. Evidence for detrital remanent magnetization carried by hematite in Devonian red beds from Spitsbergen: palaeomagnetic implications. Geophys. J. Int. 79, 573–588.
Marshall, M., Cox, A., 1971. Effect of oxidation on the natural remanent magnetization of titanomagnetite in suboceanic basalt. Nature 230, 28–31.
McCabe, C., Elmore, R.D., 1989. The occurrence and origin of Late Paleozoic remagnetization in the sedimentary rocks of North America. Rev. Geophys. 27, 471–494.
McClelland-Brown, E., 1982. Discrimination of TRM and CRM by blocking-temperature spectrum analysis. Phys. Earth Planet. Inter. 30, 405–414.
McClelland, E., 1996. Theory of CRM acquired by grain growth, and its implications for TRM discrimination and palaeointensity determination in igneous rocks. Geophys. J. Int. 126, 271–280.
Michel, F.M., Barrón, V., Torrent, J., Morales, M.P., Serna, C.J., Boily, J.F., Liu, Q., Ambrosini, A., Cismasu, A.C., Brown, G.E., 2010. Ordered ferrimagnetic form of ferrihydrite reveals links among structure, composition, and magnetism. Proc. Natl. Acad. Sci. USA 107, 2787–2792.
Mitra, R., Tauxe, L., 2009. Full vector model for magnetization in sediments. Earth Planet. Sci. Lett. 286, 535–545.
O'Reilly, W., 1984. Rock and Mineral Magnetism. Blackie Son Limited, Bishopbriggs, Glasgow.
Özdemir, Ö., Dunlop, D.J., 1993. Chemical remanent magnetization during gamma-FeOOH phase transformations. J. Geophys. Res. 98, 4191–4198.

Robb, G.L., 1949. Red bed coloration. J. Sediment. Res. 19, 99–103.
Schwertmann, U., Cornell, R.M., 2000. Iron Oxides in the Laboratory. Wiley Online Library.
Stacey, F., Banerjee, S., 1974. The Physical Principles of Rock Magnetism. Elsevier Sci. Publ. Comp., Amsterdam.
Stearns, C., Van der Voo, R., 1987. A paleomagnetic reinvestigation of the Upper Devonian Perry Formation: evidence for Late Paleozoic remagnetization. Earth Planet. Sci. Lett. 86, 27–38.
Steiner, M.B., 1983. Detrital remanent magnetization in hematite. J. Geophys. Res. 88, 6523–6539.
Stokking, L.B., Tauxe, L., 1987. Acquisition of chemical remanent magnetization by synthetic iron oxide. Nature 327, 610–612.
Stokking, L., Tauxe, L., 1990a. Properties of chemical remanence in synthetic hematite: testing theoretical predictions. J. Geophys. Res. 95, 12639–12652.
Stokking, L.B., Tauxe, L., 1990b. Multicomponent magnetization in synthetic hematite. Phys. Earth Planet. Inter. 65, 109–124.
Tan, X., Kodama, K.P., Chen, H., Fang, D., Sun, D., Li, Y., 2003. Paleomagnetism and magnetic anisotropy of Cretaceous red beds from the Tarim basin, northwest China: evidence for a rock magnetic cause of anomalously shallow paleomagnetic inclinations from central Asia. J. Geophys. Res. 108 (B2), 2107. http://dx.doi.org/10.1029/2001JB001608.
Tan, X., Kodama, K.P., Gilder, S., Courtillot, V., 2007. Rock magnetic evidence for inclination shallowing in the Passaic Formation red beds from the Newark basin and a systematic bias of the Late Triassic apparent polar wander path for North America. Earth Planet. Sci. Lett. 254 (3–4), 345–357.
Tauxe, L., Kent, D.V., Opdyke, N.D., 1980. Magnetic components contributing to the NRM of Middle Siwalik red beds. Earth Planet. Sci. Lett. 47, 279–284.
Tauxe, L., Opdyke, N.D., 1982. A time framework based on magnetostratigraphy for the Siwalik sediments of the Khaur Area, Northern Pakistan. Palaeogeogr. Palaeoclimatol. Palaeoecol. 37, 43–61.
Tauxe, L., Kent, D.V., 1984. Properties of a detrital remanence carried by haematite from study of modern river deposits and laboratory redeposition experiments. Geophys. J. R. Astron. Soc. 76, 543–561.
Tauxe, L., Kent, D.V., 2004. A simplified statistical model for the geomagnetic field and the detection of shallow bias in paleomagnetic inclinations: was the ancient magnetic field dipolar? In: Timescales of the Paleomagnetic Field, pp. 101–115.
Tauxe, L., Gee, J., Steiner, M., Staudigel, H., 2013. Paleointensity results from the Jurassic: new constraints from submarine basaltic glasses of ODP Site 801C. Geochem. Geophys. Geosyst. 14 (10), 4718–4733.
Torrent, J., Schwertmann, U., 1987. Influence of hematite on the color of red beds. J. Sediment. Res. 57, 682–686.
Van der Voo, R., Torsvik, T.H., 2012. The history of remagnetization of sedimentary rocks: deceptions, developments and discoveries. Geol. Soc. (Lond.) Spec. Publ. 371 (1), 23–53.
Van Houten, F.B., 1968. Iron oxides in red beds. Geol. Soc. Am. Bull. 79, 399–416.
Van Houten, F.B., 1973. Origin of red beds: a review—1961–1972. Annu. Rev. Earth Planet. Sci. 1, 39–61.
Walker, T.R., 1967. Color of recent sediments in tropical Mexico: a contribution to the origin of red beds. Bull. Geol. Soc. Am. 78, 917–920.
Walker, T.R., Larson, E.E., Hoblitt, R.P., 1981. Nature and origin of hematite in the moenkopi formation (Triassic), Colorado Plateau: a contribution to the origin of magnetism in red beds. J. Geophys. Res. 86 (B1), 317–333.
Wang, Z., Van der Voo, R., 1993. Pervasive remagnetization of Paleozoic rocks acquired at the time of Mesozoic folding in the South China Block. J. Geophys. Res. 98, 1729–1741.
Whidden, K.J., Lund, S.P., Bottjer, D.J., Champion, D., Howell, D.G., 1998. Paleomagnetic evidence that the central block of Salinia (California) is not a far-traveled terrane. Tectonics 17, 329–343.
Yan, M., Van der Voo, R., Fang, X.M., Parés, J.M., Rea, D.K., 2006. Paleomagnetic evidence for a mid-Miocene clockwise rotation of about 25° of the Guide Basin area in NE Tibet. Earth Planet. Sci. Lett. 241, 234–247.